Detecting traveling ionospheric disturbances with LSTM deep learning anomaly detection and GNSS
Case study: 2023 Kahramanmaras earthquake sequence

Fiona Luhrmann[*,1], J. Park[1], W-K. Wong[1], L. Martire[2], S. Krishnamoorthy[2] and A. Komjáthy[2]

[1]College of Engineering, Oregon State University, Corvallis, OR, USA , [2]Jet Propulsion Laboratory, California Institute of Technology, Pasadena, CA, USA

Abstract

Global Navigation Satellite System (GNSS) derived Total Electron Content (TEC) measurements of the ionosphere show acoustic-gravity wave disturbances, known as traveling ionospheric disturbances (TID), after seismic events. **Our work aims to develop a near-real time ionosphere anomaly detection method that can detect seismically induced TID** and incorporate this method into the GUARDIAN system developed by Jet Propulsion Laboratory. Our method uses a Long Short Term Memory (LSTM) neural network to detect anomalous behavior in the ionosphere and filters these to similar anomalous wave characteristics in a localized region. This method successfully detected TID 10 minutes after the M7.5 earthquake on February 6, 2023 in southern Turkey.

Observation of seismically induced TID with GNSS has been proven by extensive studies using TEC measurements from GNSS observation data to detect acoustic-gravity wave disturbance within the ionosphere after earthquake events such as the March 11, 2011 (UTC) Tohoku earthquake (Occhipinti et al., 2013) (Rolland et al., 2011), and the July 4, 2019 (UTC) Ridgecrest earthquake (Sanchez et al., 2022).

Project Assumptions

- Gravity wave frequencies range 1 - 3 mHz, acoustic waves $\gtrsim$ 4 mHz, and overall prominent waves $\leq$ 10 mHz (Matoza et al., 2022).
- Deep learning neural networks capture the temporal dynamics of the ionosphere.
- Ionospheric anomalies will deviate largely from predicted TEC more than once in a small window of time.
- During a TID, local TEC measurements will come into phase synchrony as the wave passes.

Data Processing

GNSS signal differential delay measures Slant Total Electron Content (Slant TEC) in units $10^{16} el/m^2$. Slant TEC data is filtered with the fourth-order Butterworth high pass filter, removing frequencies below 1.1 mHz (Martire et al., 2022).

$$\text{Slant TEC} \approx \frac{f_1^2 f_2^2}{K(f_1^2 - f_2^2)}(\phi_{f_1} - \phi_{f_2})$$

K is a constant, approximating the plasma frequency ($\approx 40.308193 m^3 s^{-2}$), $f_{1,2}$ are the carrier frequencies, and $\phi_{1,2}$ are the measured phases along the respective frequencies (Teunissen and Montenbruck, 2017)

References

Gers, F. A., Schmidhuber, J., and Cummins, F. (2000). Learning to forget: Continual prediction with lstm. *Neural computation*, 12(10):2451–2471.

Martire, L., Krishnamoorthy, S., Vergados, P., Romans, L. J., Szilágyi, B., Meng, X., Anderson, J. L., Komjáthy, A., and Bar-Sever, Y. E. (2022). The guardian system-a gnss upper atmospheric real-time disaster information and alert network. *GPS Solutions*, 27(1):1521–1886.

Matoza, R. S., Fee, D., Assink, J. D., Iezzi, A. M., Green, D. N., Kim, K., Toney, L., Lecocq, T., Krishnamoorthy, S., Lalande, J.-M., Nishida, K., Gee, K. L., Haney, M. M., Ortiz, H. D., Brissaud, Q., Martire, L., Rolland, L., Vergados, P., Nippress, A., Park, J., Shani-Kadmiel, S., Witsil, A., Arrowsmith, S., Caudron, C., Watada, S., Perttu, A. B., Taisne, B., Mialle, P., Le Pichon, A., Vergoz, J., Hupe, P., Blom, P. S., Waxler, R., De Angelis, S., Snively, J. B., Ringler, A. T., Anthony, R. E., Jolly, A. D., Kilgour, G., Averbuch, G., Ripepe, M., Ichihara, M., Arciniega-Ceballos, A., Astafyeva, E., Ceranna, L., Cevuard, S., Che, I.-Y., De Negri, R., Ebeling, C. W., Evers, L. G., Franco-Marin, L. E., Gabrielson, T. B., Hafner, K., Harrison, R. G., Komjathy, A., Lacanna, G., Lyons, J., Macpherson, K. A., Marchetti, E., McKee, K. F., Mellors, R. J., Mendo-Perez, G., Mikesell, T. D., Munaibari, E., Oyola-Merced, M., Park, I., Pilger, C., Ramos, C., Ruiz, M. C., Sabatini, R., Schwaiger, H. F., Tailpied, D., Talmadge, C., Vidot, J., Webster, J., and Wilson, D. C. (2022). Atmospheric waves and global seismoacoustic observations of the january 2022 hunga eruption, tonga. *Science (American Association for the Advancement of Science)*, 377(6601):95–100.

Occhipinti, G., Rolland, L., Lognonné, P., and Watada, S. (2013). From sumatra 2004 to tohoku-oki 2011: The systematic gps detection of the ionospheric signature induced by tsunamigenic earthquakes. *Journal of Geophysical Research: Space Physics*, 118(6):3626–3636.

Rolland, L. M., Lognonné, P., Astafyeva, E., Kherani, E. A., Kobayashi, N., Mann, M., and Munekane, H. (2011). The resonant response of the ionosphere imaged after the 2011 off the pacific coast of tohoku earthquake. *Earth, planets, and space*, 63(7):853–857.

Sanchez, S. A., Kherani, E. A., Astafyeva, E., and de Paula, E. R. (2022). Ionospheric disturbances observed following the ridgecrest earthquake of 4 july 2019 in california, usa. *Remote sensing (Basel, Switzerland)*, 14(1):188–.

Teunissen, P. and Montenbruck, O. (2017). *Springer Handbook of Global Navigation Satellite Systems*. Springer Handbooks. Springer International Publishing, Cham, 1st ed. 2017. edition.

Ionospheric Anomaly Detection Methodology

Three main components based on project assumptions:

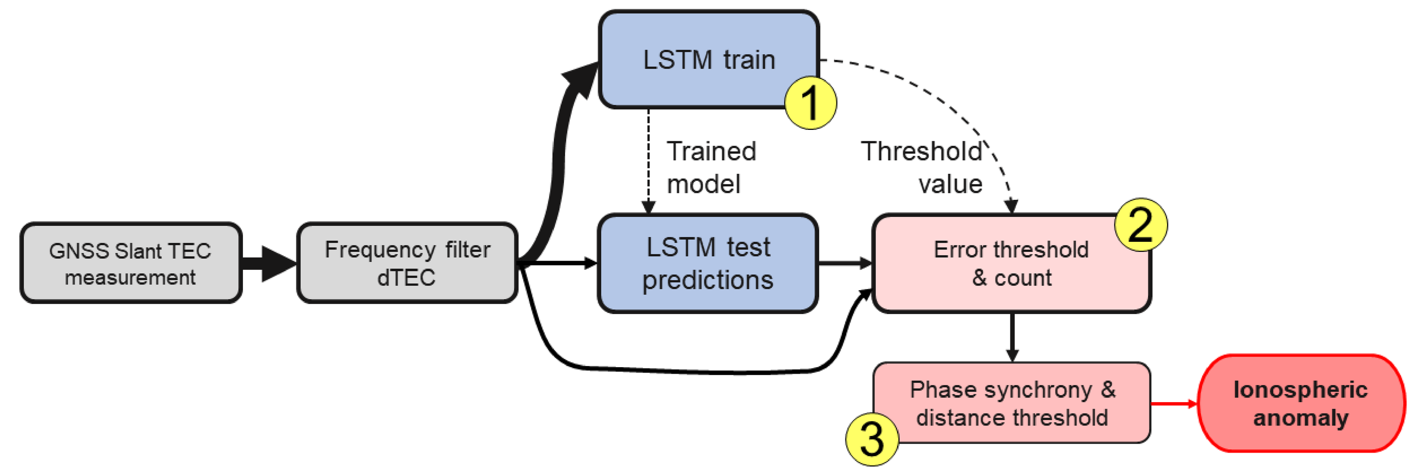

Figure 1: Process flow diagram for ionospheric anomaly detection method

1) Long Short Term Memory (LSTM), a recurrent neural network

Training and testing an LSTM to output TEC predictions.

LSTM Training Parameters

- **A** is an LSTM cell with forget gate (Gers et al., 2000).
- Input time series of length 60, output prediction time series of length 1
- Minimization of the mean square error loss during validation
- 25 epochs for training
- Batch size of 64

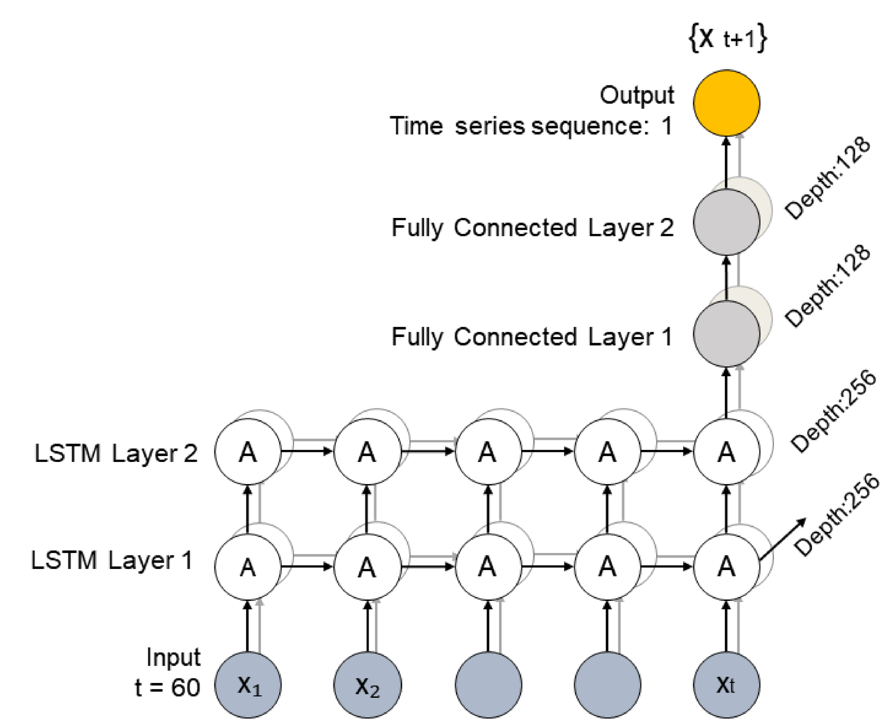

Figure 2: LSTM architecture.

2) Error thresholding and count

Error thesholding, which filters errors (MSE = measured TEC minus TEC predictions)^2, outside of the normal distribution of errors and **error count**, which filters for clusters of errors within a window of time.

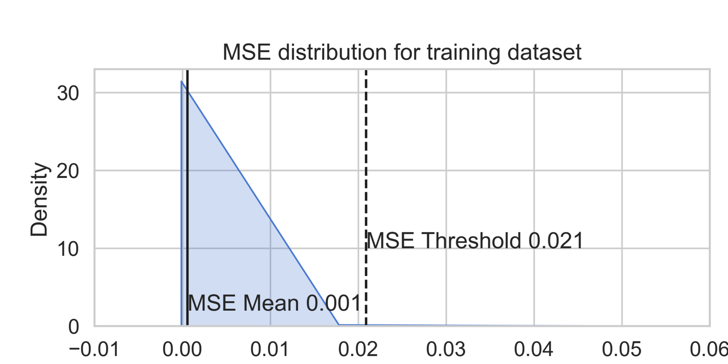

Figure 3: Case Study example: Setting the MSE threshold with the MSE distribution from the training data set

- Error threshold = Training set MSE mean + 3x MSE standard deviation (Case study example 0.021 $TECU^2$).
- Error count > 3 within a window of 24 (e.g., 2 min at 5 sec sample rate).

3) Phase synchrony and distance thresholding

Phase synchrony, a pair-wise check between TEC measurements for similar wave frequencies and phases, and **distance thresholding**, to reduce results to localized disturbances.

- φ_{ij} phase synchrony, $h(x_i)$ $h(x_j)$ Hilbert Transforms of the station dTEC values.
- Signals with phase synchrony measures ≥ 0.9 within 200km (Ionospheric Pierce Point (IPP) distance) of each other are identified as an ionospheric anomaly.

$$\varphi_{ij} = 1 - \sin\left(\frac{|h(x_i) - h(x_j)|}{2}\right) \qquad (1)$$

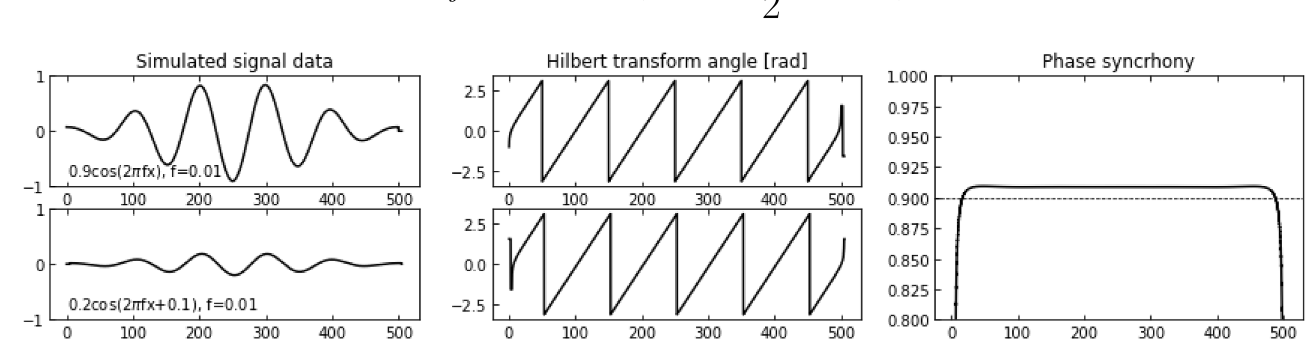

Figure 4: Phase synchrony example on simulated cosine functions

2023 Kahramanmaras earthquake sequence

On February 6, 2023, at 01:17:34 (UTC), a magnitude 7.8 earthquake occurred in southern Turkey near the northern border of Syria, from a strike-slip fault at a depth of 10.0 km. Nine hours later, at 10:24:48 (UTC) a magnitude 7.5 earthquake, located 95 km to the northeast of the first, occurred at a depth of 7.4 km. Both occurred within the area of the junction between the Anatolia, Arabia, and Africa plates (earthquake.usgs.gov).

Set up

- 7 stations in the region maintained by GUARDIAN Martire et al. (2022). Satellite constellations GPS, Galileo, GLONASS, and BeiDou.
- **10-minute data streaming with 5 minute overlap for near real time detection.**
- **LSTM Training Data:** December 1, 2022 through January 31, 2023 from 3 stations (DYNC, GRAC, and NICO) and 4 satellites (C201M, E203, GPS50, R856), creating 12 'hub' models. This method is used for scalability and efficiency.
- **LSTM Testing Data:** First week of February 2023, 734 station-satellite signals were tested.

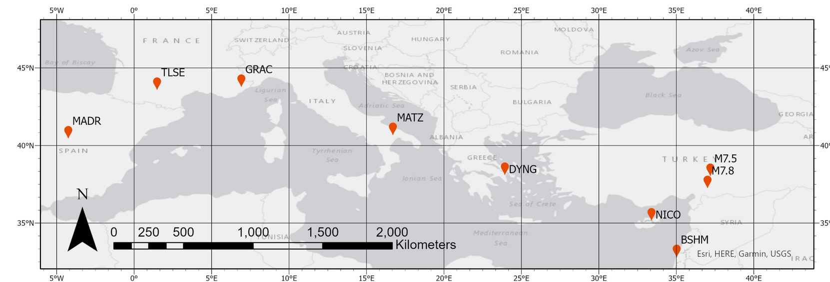

Figure 5: Map of the station locations and the 2023 Kahramanmaras M7.8 and M7.8 earthquake epicenters.

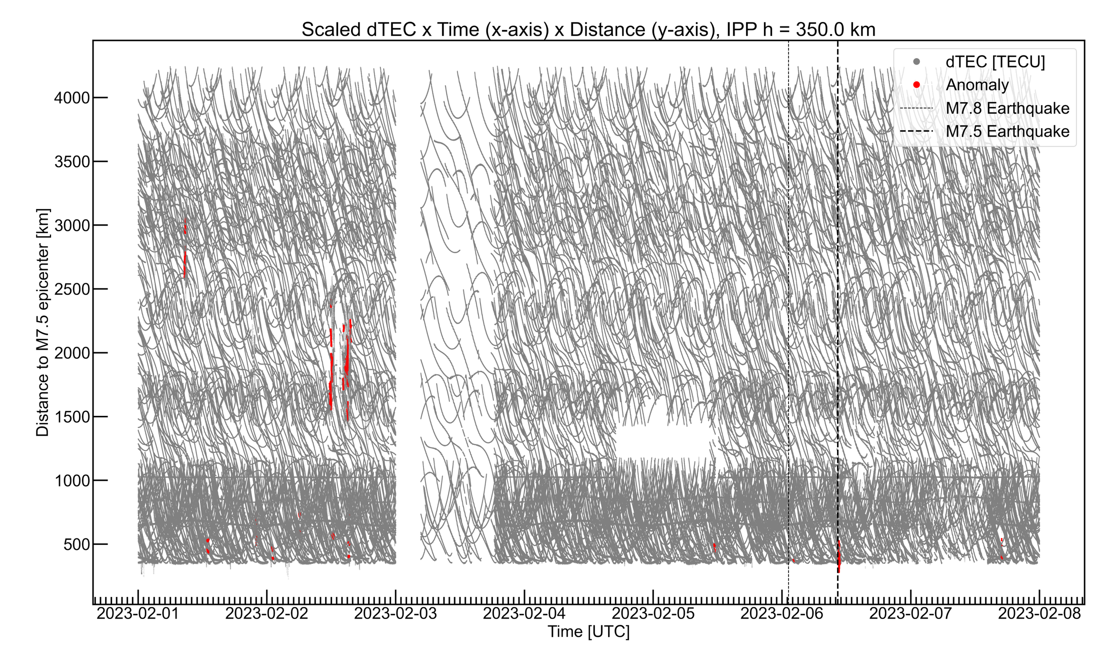

Figure 6: Ionospheric anomaly detection results over the first week of February, 2023. False positives are evident in the first two days during signal disturbances.

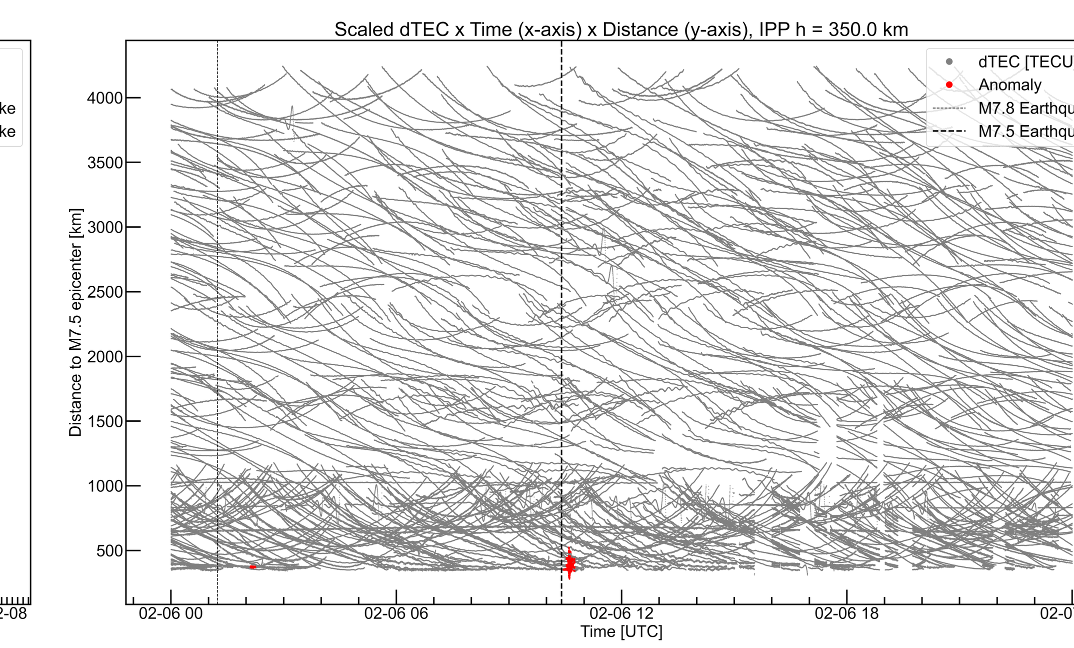

Figure 7: Ionospheric anomaly detection results on February 6, 2023, the day of the earthquake sequence.

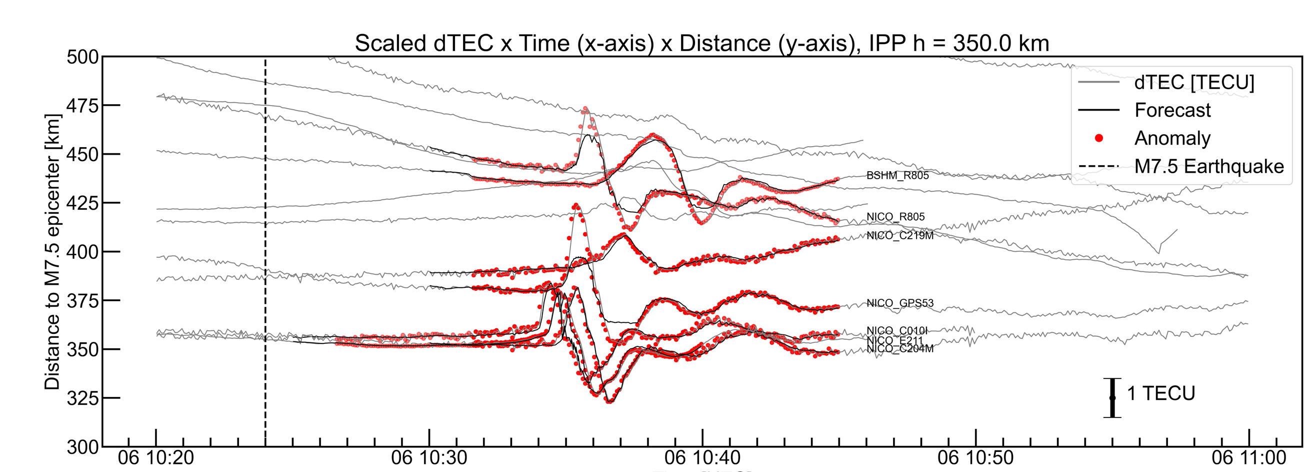

Figure 8: Detail of the ionospheric anomaly detection after the M7.5 earthquake. The anomaly detection method identifies the entire 10 minute window as an anomaly event for further analysis.

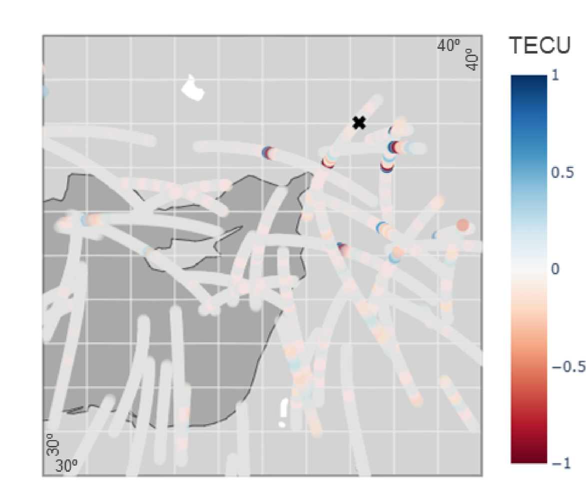

Figure 9: Map of IPP at 350km, colored with TEC between hours of 10:20 to 11:00 UTC on February 6, 2023. The black 'x' symbol is the epicenter of the M7.5 earthquake.

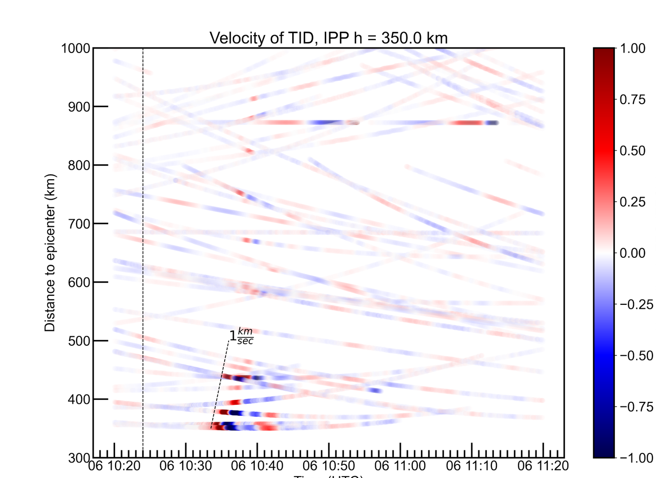

Figure 10: Approximate velocity of the detected first arrival wave is $1\frac{km}{sec}$, in line with previous research observations of seismic induced TID.

Results

- **Detected seismically induced TID** starting at 10:34 (UTC), 10 minutes after the M7.5 earthquake at 10:24 (UTC). 7 signals were identified as anomalous across 2 stations and 6 satellites.
- The 10:34 (UTC) disturbance was within range of $\sim$[-2,2] TECU.
- The 10:34 (UTC) disturbance has similar characteristics of velocity ($1\frac{km}{sec}$) and frequency (gravity waves $\leq 4mHz$) of previously studied seismic induced disturbances in the ionosphere.
- 11 false positives were also detected across the week. 2 due to signal disruptions and 9 due to minor, synchronous perturbations of an unknown source at this time.
- There was no detection after the M7.8 earthquake.

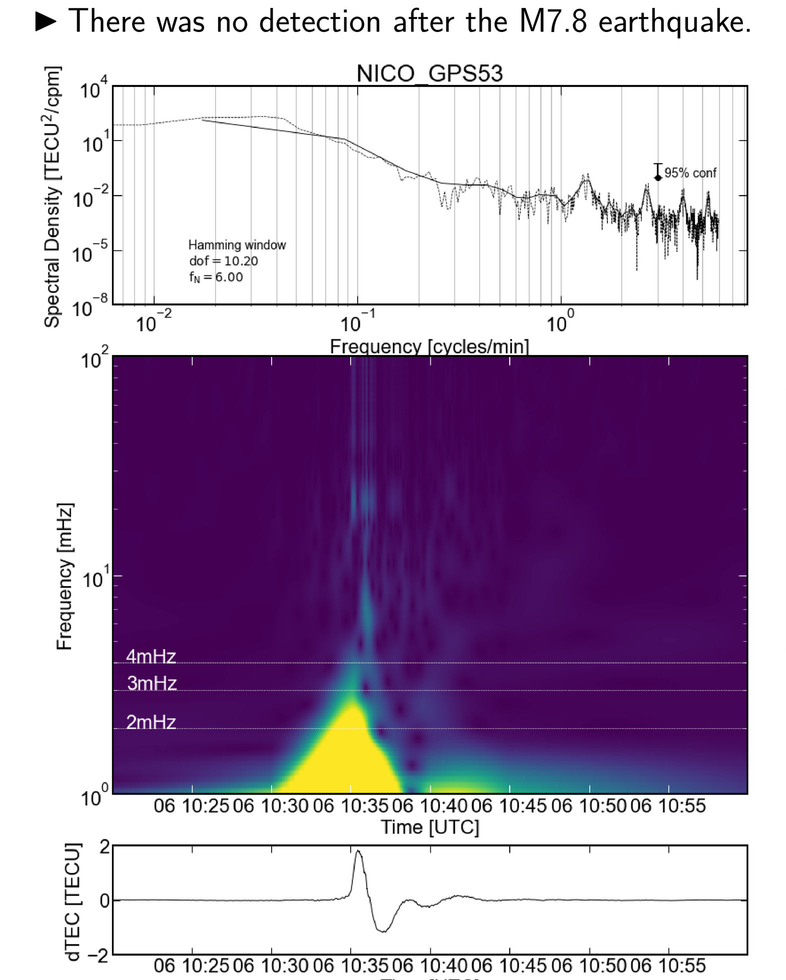

Figure 11: Power spectral density and wavelet analysis (Morlet) of the dTEC measurement between station NICO and GPS SVN 53.

Conclusion

Successful detection of seismic induced acoustic-gravity wave disturbances in the ionosphere with streaming data show that the project assumptions hold and are an effective method for ionospheric monitoring in near real time. There is still more work to do to reduce false positive detection due to signal disruptions which will continue in near real time environments.

Acknowledgements

This work was supported by NASA Jet Propulsion Laboratory.

Future Work:

- Expand ionospheric anomaly detection to tsunami events.
- Develop a method to classify detected ionospheric anomalies.
- Improve detection methodology to reduce false positives.

*Fiona Luhrmann <luhrmanf@oregonstate.edu>